JOURNAL OF AIRCRAFT
Vol. 44, No. 3, May–June 2007

Study on the Induced Velocity and Noise Characteristics of a Scissors Rotor

Guo-Hua Xu,* Qi-Jun Zhao,† and Yan-Hui Peng‡
National Key Laboratory of Rotorcraft Aeromechanics, Nanjing University of Aeronautics and Astronautics, 210016 Nanjing, People's Republic of China

DOI: 10.2514/1.24460

Aerodynamic and acoustic experiments were carried out to investigate the induced inflow distribution and noise characteristics of a scissors rotor in hover. The aerodynamic experiment was conducted on a model rotor rig and the induced inflows for two different scissors rotor configurations (the L configuration and U configuration) were measured. The experimental results indicate that the induced velocity near the lower blades is consistently larger than that near the upper blades. A free-wake analysis was used to predict the aerodynamic characteristics. The variation of the induced velocity with different scissors angles was simulated analytically and the results were compared with test data. The acoustic experiment was conducted in an anechoic aeroacoustic laboratory and the noise levels for both the scissors rotor configuration and a conventional configuration were measured. The effects of different scissors angles on rotor noise were investigated. It was shown that the noise level of a scissors rotor depends on both the azimuthal and vertical spacing and is not necessarily less than that of a conventional configuration.

Nomenclature

$\boldsymbol{R}(\phi, \psi)$	=	location vector of a collocation point on vortex filaments
$\boldsymbol{v}$	=	induced velocity
x, y, z	=	rotor hub coordinate system
ΔH	=	vertical separation of scissors rotor
θ_7	=	collective pitch angle
ϕ	=	wake age
$\psi(t)$	=	azimuthal angle
Ω	=	rotor rotational angular speed

Subscripts

j, k	=	grid indices

Superscript

n	=	number of iteration

I. Introduction

THE scissors rotor configuration has been employed on modern armed helicopters such as the AH-64 helicopter as a tail rotor [1]. The main characteristic of a scissors rotor configuration is that it consists of two pairs of rotor blades with scissors angle and vertical separation, which is clearly different from a conventional rotor configuration. The scissors angle and vertical separation of the scissors rotor configuration significantly change the position and strength of the tip vortices shed from upper and lower blades, which in turn changes the aerodynamic and acoustic characteristics of the rotor [2]. There is a lot of documented research on the aerodynamics and acoustics of conventional rotors, but only a limited number of such investigations for the scissors (tail) rotor [3,4].

In this paper, both aerodynamic and acoustic experiments were carried out to investigate the induced inflow and noise characteristics of a model scissor rotor. In the aerodynamic experiment, the induced inflow distributions across the scissors rotor were measured using the 3-D laser Doppler velocimetry (LDV). The two different scissors rotor configurations tested are the L configuration, in which the lower pair of blades are leading the upper pair of blades, and the U configuration, in which the upper pair of blades are leading the lower pair of blades.

An analytical method based upon the rotor free-wake model and the blade second-order lifting-line model is also presented for calculating the induced velocity of a scissors rotor. Using the method, the time-averaged induced velocities near the upper and lower pairs of blades were calculated for the scissors rotor configuration and compared with the measured results from experiments.

It was claimed that the advantage of using a nonuniform blade azimuthal spacing (scissors layout) is its improvement in noise characteristics, which comes from the so-called modulated effects [5,6]. However, whether a scissors (tail) rotor, which includes not only nonuniform blade azimuthal spacing but also vertical separation, can indeed reduce the noise level is doubtful or controversial. Introducing the vertical separation may lead to strong blade-vortex interactions, which can offset the benefit from the nonuniform azimuthal spacing. In this study, to fully understand the noise characteristics of a scissors rotor configuration, an experimental investigation on the scissors rotor noise was also performed in an anechoic aeroacoustic laboratory of the Nanjing University of Aeronautics and Astronautics (NUAA). The noise characteristics of the scissors rotor and the conventional rotor were investigated and compared with each other. Also, the effects of the scissors angle and tip Mach number on rotor noise were examined.

II. Experimental Investigation of Scissors Rotor Aerodynamics

A. Description of Experiments

To investigate the effects of scissors rotor configuration on the induced velocity distribution, the experiment was carried out using a model scissors rotor on a 2-m rotor rig at NUAA by a 3-D LDV (Fig. 1). Two different configurations of the scissors rotor were investigated, that is, the L configuration and U configuration as mentioned in the introduction.

The model rotor consists of a pair of coaxial two-bladed rotors, as shown in Fig. 1. The rotor blades have a rectangular planform with untwisted NACA-0015 airfoil. The rotor diameter and blade chord length are 2.0 and 0.06 m, respectively. The model rotor is installed

Received 5 April 2006; revision received 13 December 2006; accepted for publication 7 January 2007.

*Professor, PO Box 331; ghxu@nuaa.edu.cn.
†Lecturer, PO Box 331; zhaoqijun@nuaa.edu.cn.
‡Graduate Student, PO Box 331.

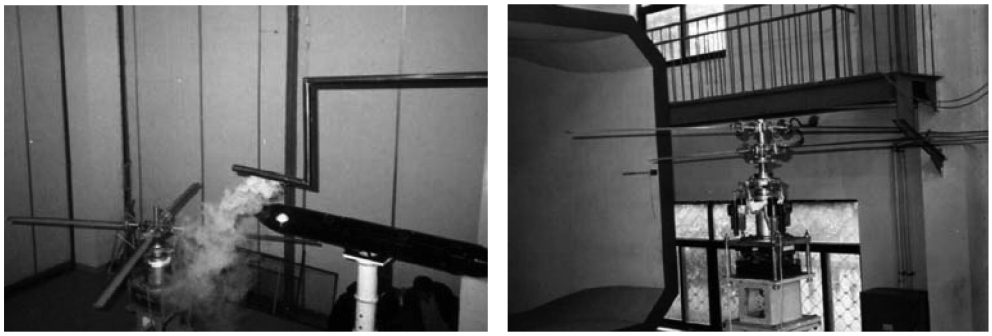

Fig. 1 Experiment setup for measurement of induced velocities of scissors rotor on a rotor rig.

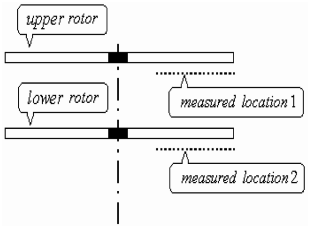

Fig. 2 Schematic of measured points.

2.6 m above the ground and is operated at an angular velocity of 1200 rpm. In the experiments, the scissors angle can be chosen among $\Delta\psi_s = 0$, 30, 45, 60, and 90 deg, and the vertical separation between the two pair of rotors can be chosen to be $\Delta\bar{H} = H/R = 0.10$ and 0. As a special case of the scissors rotor configuration, the conventional rotor configuration is recovered with $\Delta\bar{H} = 0$ and $\Delta\psi_s = 90$ deg. The measurement locations for the induced velocities are schematically shown in Fig. 2.

B. Experimental Results

Figure 3 presents a typical measured time-averaged induced velocity distribution near the upper and lower rotor blades for the L and U scissors configurations at a scissors angle of $\Delta\psi_s = 30$ deg and a vertical separation of $\Delta\bar{H} = 0.10$. In the plots, "Upper" denotes the results obtained at the measurement location 1 (see Fig. 2), which is near the blades of the upper rotor, and "Lower" denotes the results measured at the measurement location 2, which is near the blades of the lower rotor. As shown in Fig. 3, the induced velocity near the lower rotor blades is consistently larger than that near the upper rotor blades for both configurations except at the tip region. This suggests that the contracted wake shed from the upper rotor induces higher inflow on the lower rotor. Similar results were obtained for the other scissors angles. Therefore, they are not presented here.

III. Theoretical Analysis of the Induced Velocity for the Scissors Rotor

Unlike a conventional configuration, which has a zero vertical separation and a uniform azimuthal blade spacing, a scissors configuration has both a blade azimuthal spacing and vertical separation, which will substantially change the location and strength of wake vortices shed behind the blades of the upper and lower rotors, and provide higher blade-vortex encounter possibility [2]. For such a highly complicated vortical flowfield, the free-wake method may be a proper analytical tool. The free-wake analysis for a conventional rotor has been documented in [7–12]. For the scissors rotor configuration, the free wake for the upper and lower rotor is evolved in their own coordinate frames and the effect of their mutual interactions is treated as additional source terms on the governing convection equation.

A. Solution of Free Wake

The rotor hub coordinate frame is used to define the wake geometry. As shown in Fig. 4, y axis is along the angular velocity vector and the axes x and z are in the rotational plane. A typical vortex filament shed from the rotor blade can be geometrically described as a space curve $\boldsymbol{R}(\phi, \psi)$ in the reference system, where ψ is blade azimuthal angle and ϕ is a measure of the age of collocation points of a vortex filament. The governing convection equation [8] describing the evolution of a vortex filament can be expressed as

$$\frac{\partial \boldsymbol{R}(\phi,\psi)}{\partial \phi} + \frac{\partial \boldsymbol{R}(\phi,\psi)}{\partial \psi} = \frac{1}{\Omega}\boldsymbol{v}[\boldsymbol{R}(\phi,\psi)] \tag{1}$$

where $\boldsymbol{v}$ is the total induced velocity at the collocation point, which includes the effect from the other pair of rotor.

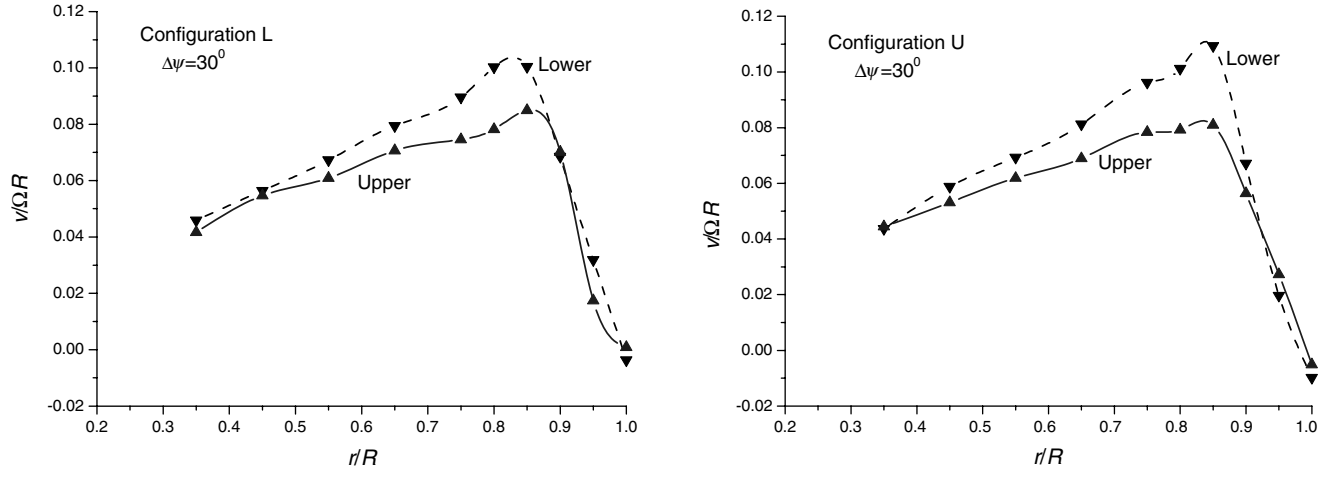

Fig. 3 Measured time-averaged induced velocity distributions near upper and lower blades.

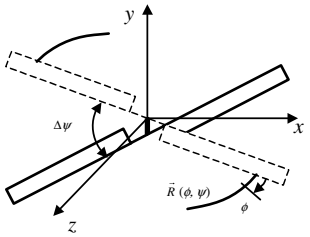

Fig. 4 Schematic of coordinate system.

A five-point finite difference scheme [8] with equal step size in the space and time, that is, $\Delta\psi = \Delta\phi$, was used to solve the governing equation. Equation (1) can be written in a finite difference form as

$$4\Omega[\boldsymbol{R}(\phi_j, \psi_k) - \boldsymbol{R}(\phi_{j-1}, \psi_{k-1})] = \Delta\psi\{\boldsymbol{v}(\phi_j, \psi_k) + \boldsymbol{v}(\phi_{j-1}, \psi_k) + \boldsymbol{v}(\phi_j, \psi_{k-1}) + \boldsymbol{v}(\phi_j, \psi_{k-1}) + \boldsymbol{v}(\phi_{j-1}, \psi_{k-1})\} \quad (2)$$

The initial condition of Eq. (2) is that the vortex filament leaves the blade trailing edge at each initial instant, and a periodic boundary condition is used:

$$\boldsymbol{R}(\phi, 2\pi + \psi) = \boldsymbol{R}(\phi, \psi) \quad (3)$$

Equation (2) is an implicit equation and is solved using the pseudoimplicit predictor-corrector (PIPC) scheme of [8]. The advantage with the PIPC scheme is its good numerical characteristics [12]. The solution procedure consists of a predictor and corrector step.

Predictor:

$$\boldsymbol{R}'(\phi_j, \psi_k) = \boldsymbol{R}'(\phi_{j-1}, \psi_{k-1}) + \frac{\Delta\psi}{4\Omega}[\boldsymbol{v}^{n-1}(\phi_j, \psi_k) + \boldsymbol{v}^{n-1}(\phi_{j-1}, \psi_k) + \boldsymbol{v}^{n-1}(\phi_j, \psi_{k-1}) + \boldsymbol{v}^{n-1}(\phi_{j-1}, \psi_{k-1})] \quad (4)$$

Corrector:

$$\boldsymbol{R}^n(\phi_j, \psi_k) = \boldsymbol{R}^n(\phi_{j-1}, \psi_{k-1}) + \frac{\Delta\psi}{4\Omega}[\boldsymbol{v}'(\phi_j, \psi_k) + \boldsymbol{v}'(\phi_{j-1}, \psi_k) + \boldsymbol{v}'(\phi_j, \psi_{k-1}) + \boldsymbol{v}'(\phi_{j-1}, \psi_{k-1}) + \boldsymbol{v}'(\phi_{j-1}, \psi_{k-1})] \quad (5)$$

Also, the aerodynamics of each rotor blade is modeled using the second-order lifting-line theory. In this model, the blade is divided into a finite number of spanwise segments with the spanwise bound vortex located at the 1/4-chord line and the control point placed at the 3/4-chord line in each segment. The wake vortex filaments are shed from the blade trailing edges. The bound circulation is solved by applying the zero-normal flow condition at each control point. Because the whole system is a highly nonlinear system, the blade aerodynamic and the wake model are coupled through the solution of the bound circulation and iterated until a convergent solution is obtained.

Fig. 6 Noise experiments on scissors rotor in anechoic aeroacoustic laboratory.

B. Comparison of Calculated and Measured Results

By using the free method analysis described in the preceding section, the induced velocity distributions for L and U scissors rotor configurations at different scissors angles are calculated and compared with the corresponding experimental results. Figure 5 shows a typical comparison between the calculated and measured induced velocity distributions at a scissors angle of $\Delta\psi_s = 60$ deg and a vertical separation of $\Delta\bar{H} = 0.10$. It can be clearly seen from the figure that the results calculated with the proposed model correlates well with the experimental data for both configurations L and U.

IV. Experimental Investigations of the Scissors Rotor Acoustics

A. Description of Experiment

The noise experiments were conducted in the anechoic aeroacoustic laboratory of NUAA (Fig. 6). The laboratory has a net space of $5.0 \times 3.8 \times 4.0$ m and a good anechoic ability with a background noise of 13.5 dBA.

The model rotor used in the noise experiments was the same as one used in the aerodynamic experiments of Sec. II. To avoid the recirculating wake flow and make use of available exhaust channel in the laboratory, the rotor axis was laid horizontally on the test rig [13].

The observation points were distributed in the rotor plane and under the rotor plane with different distance from the hub center as shown in Fig. 7.

In the present acoustic experiments, the discrete sample data during a time interval T were obtained by a set of measurement instruments [13], and used a discrete Fourier transform (DFS) on aperiodic signals to get a frequency analysis. In the measurement

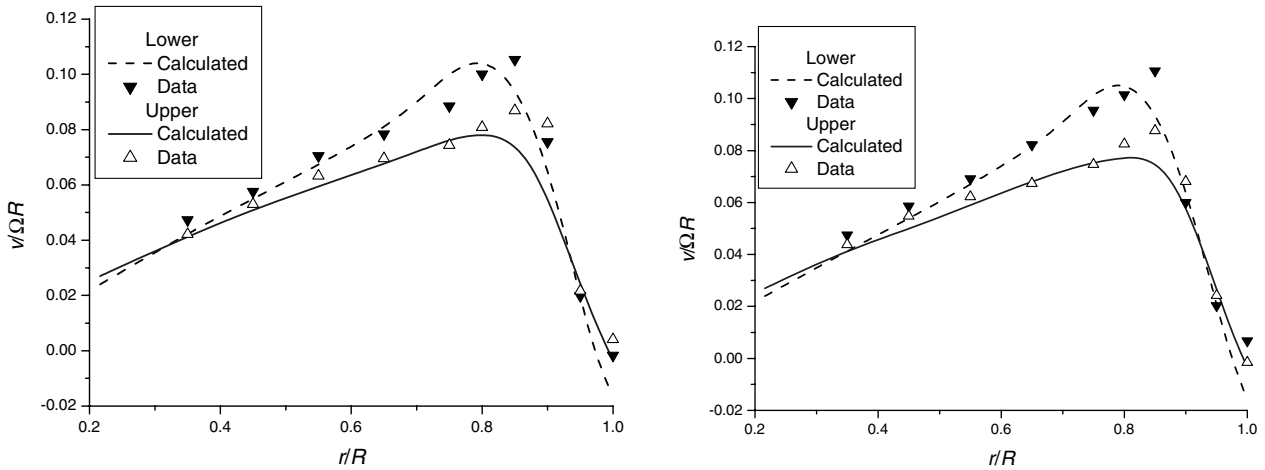

a) Configuration L **b) Configuration U**

Fig. 5 Calculated time-averaged induced velocities and comparisons with experimental data.

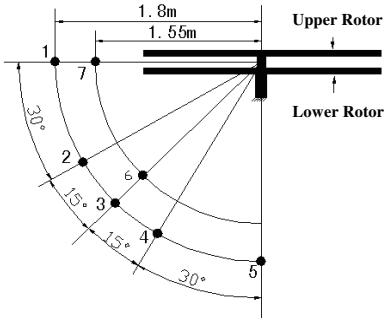

Fig. 7 Distribution of observing points.

instruments, the DFS frequency analysis was included and the DFS actually regards the aperiodic signals as the periodic signals with the periodic time of ∞.

B. Experimental Results

1. Noise Comparisons Between Unconventional and Conventional Rotor Configurations

The noise experiments were carried out to investigate the noise characteristics of an unconventional rotor configuration.

Table 1 shows the total noise level expressed in terms of dBA measured at the observation points for the configuration with a scissors angle of 90 deg and two different vertical separations. The rotor operates with a collective pitch of $\theta_7 = 10$ deg and a rotational speed of 1000 rpm. In the table, $\Delta\bar{H} = 0$ and $\Delta\bar{H} = 0.1$ correspond to the conventional and unconventional configurations, respectively.

In Table 1, the measured data on observation points 1, 2, 3, and 6 are presented for comparisons, but the results on observation points 4 and 5 are not included. The main reason was that these two observation points were located inside the rotor wake during experiments and the measured noise was severely affected by the rotor wake, and thus the results at these two points were suspect even if the UA0386 wind cover was added on microphones. For the operating condition in the present experiments, it can be clearly seen from Table 1 that the noise level of the unconventional configuration rotor with $\Delta\psi_s = 90$ deg and $\Delta\bar{H} = 0.1$ is always higher than that of the conventional configuration one with $\Delta\psi_s = 90$ deg and $\Delta\bar{H} = 0$. The results clearly demonstrate the importance of the vertical separation in determining the noise characteristics of scissor rotor. This can be explained that for an unconventional configuration rotor with nonzero vertical separation, the tip vortex shed from the upper rotor either passes above or below the blades of lower rotor, which indicates higher blade-vortex interaction (BVI) possibilities. However, for a conventional configuration rotor at hover condition, the tip vortex shed from the previous blade usually passes below the following blades.

Table 1 Noise comparisons between unconventional and conventional rotors at $\theta_7 = 10$ deg, dBA

Observing points	Vertical separation	
	$\Delta\bar{H} = 0$	$\Delta\bar{H} = 0.1$
Point 1	79.0	80.4
Point 2	89.4	91.4
Point 3	87.9	91.1
Point 6	90.2	92.9

It can also be seen from Table 1 that the noise level at the observation point 1 (in the rotor plane) is lower than those at the other observation points (out of the plane) and the maximum difference is approximately 10 dBA, which means that blade loading noise is greater than thickness noise for the present operating condition, which has a high thrust coefficient and a low tip Mach number.

Similarly, Figs. 8 and 9 show the time histories of the measured sound pressure and the corresponding sound pressure level (SPL) frequency spectrum for the two rotor configurations at a rotational speed of 1000 rpm and a scissors angle of $\Delta\psi_s = 90$ deg, respectively.

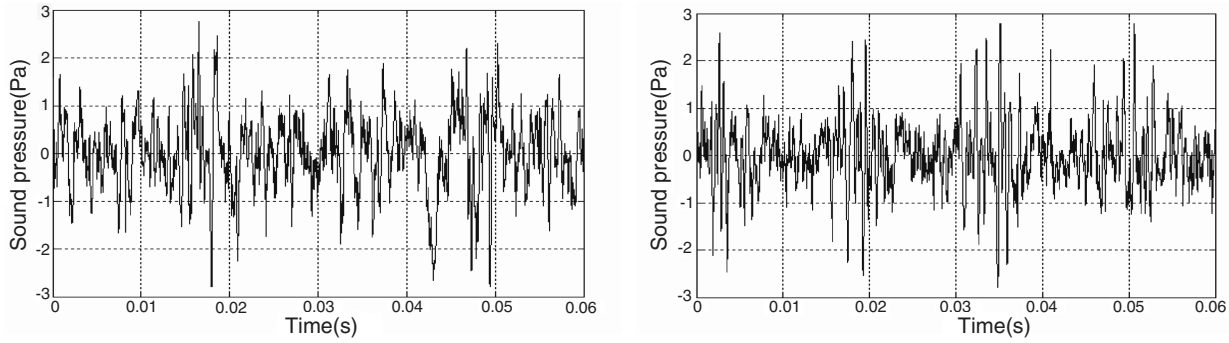

a) Unconventional rotor configuration **b) Conventional rotor configuration**

Fig. 8 Sound pressure time histories for unconventional and conventional rotors at $\theta_7 = 10$ deg (observing point 6).

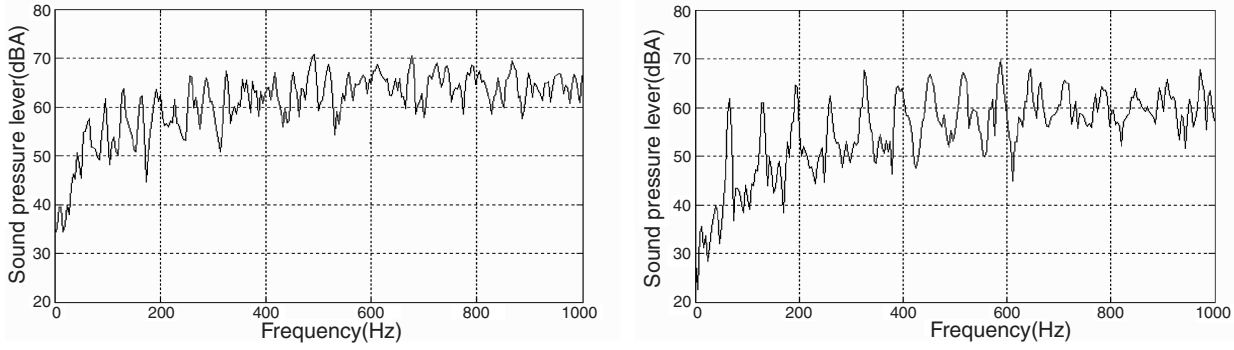

a) Unconventional rotor configuration **b) Conventional rotor configuration**

Fig. 9 Frequency spectrum for unconventional and conventional rotors at $\theta_7 = 10$ deg (observing point 6).

Table 2 Noise comparisons for different scissors angles (configuration L), dBA

Observing points	Scissors angles				
	$\Delta\psi_s = 0$ deg	$\Delta\psi_s = 30$ deg	$\Delta\psi_s = 45$ deg	$\Delta\psi_s = 60$ deg	$\Delta\psi_s = 90$ deg
Point 1	80.4	79.9	79.8	79.6	80.4
Point 2	90.8	89.6	89.4	89.7	91.4
Point 3	90.8	88.3	88.5	88.6	91.1
Point 6	92.3	90.4	90.5	91.0	92.9

Table 3 Noise comparisons for different scissors angles (configuration U), dBA

Observing points	Scissors angles		
	$\Delta\psi_s = 30$ deg	$\Delta\psi_s = 45$ deg	$\Delta\psi_s = 60$ deg
Point 1	92.7	80.1	80.6
Point 2	102.7	90.9	91.3
Point 3	102.0	90.7	91.4
Point 6	105.2	92.5	93.0

2. Effects of Scissors Angles

Table 2 is a comparison of the total rotor noise levels measured for the various scissors angle rotor configurations at $n = 1000$ rpm and $\theta_7 = 10$ deg, the vertical separation is fixed at $\Delta\bar{H} = 0.1$.

From the comparisons of noise levels for three scissors configurations with $\Delta\psi_s = 30$, 45, and 60 deg, it is shown that the variations of noise levels are not obvious with scissors angles on each observing point, which means no strong BVI phenomenon occurs for these scissors configurations. As mentioned previously, there is no difference in the layout of blades for both configuration L and configuration U when the scissors angle is equal to 0 or 90 deg. With comparisons to the rotor configurations with $\Delta\psi_s = 30$, 45, and 60 deg, the noise level for the scissors angle of 90 deg is larger on all observing points. In other words, the noise level for the uneven-spacing scissors rotor (30, 45, and 60 deg) is smaller than that of the even-spacing configuration (90 deg), and the results are consistent with the conclusions about uneven blade spacing rotor in [5,6].

Table 3 gives the total noise levels of the scissors rotor for configuration U at the condition of $\theta_7 = 10$ deg and rotation speed of 1000 rpm.

As seen from Table 3, the noise levels on the observing points for configuration U are larger when compared with configuration L, especially for the scissors angle of 30 deg, the noise value is the largest with an increment of 12 dBA. The reason causing the remarkable increase in noise level might be the strong BVI resulted from the close encounter of the tip vortex shed from the upper rotor with the lower blades. Thus the effects of scissors angles and configurations L and U on noise levels depend upon whether or not a serious BVI occurs at the operating condition. Also, the comparisons between Tables 2 and 3 indicate that the noise characteristics for configurations L and U are not identical.

Table 4 Noise comparisons for different rotor speeds (configuration L), dBA

Observing points	Rotor speed	
	$\Delta\psi_s = 45$ deg	
	1000 rpm	1200 rpm
Point 1	79.8	83.2
Point 2	89.4	93.5
Point 3	88.5	92.8
Point 6	90.4	94.9

Table 5 Noise comparisons for different rotor speeds (configuration U), dBA

Observing points	Rotor speed	
	$\Delta\psi_s = 45$ deg	
	1000 rpm	1200 rpm
Point 1	80.1	84.1
Point 2	90.9	95.4
Point 3	90.7	95.9
Point 6	92.5	96.8

Typically, Fig. 10 gives the comparisons of the sound pressure time history for configurations L and U on observing point 6 for $\Delta\psi_s = 30$ deg and $n = 1000$ rpm. As seen from the two figures, both the number of pressure impulses and the impulsive amplitudes are higher for configuration U compared with configuration L, resulting in the total noise level for configuration U to be larger.

3. Effects of Tip Mach Number

Tables 4 and 5 give the measured noise levels at the observing points for configurations L and U at scissors angle of 45 deg for rotor speeds of $n = 1000$ and 1200 rpm.

As seen from the table, the rotor noise level increases rapidly with the increase of rotor speed on each observing point for both configuration L and configuration U, and the increment is about 4 dBA when the rotor speed changes from 1000 to 1200 rpm. Indeed,

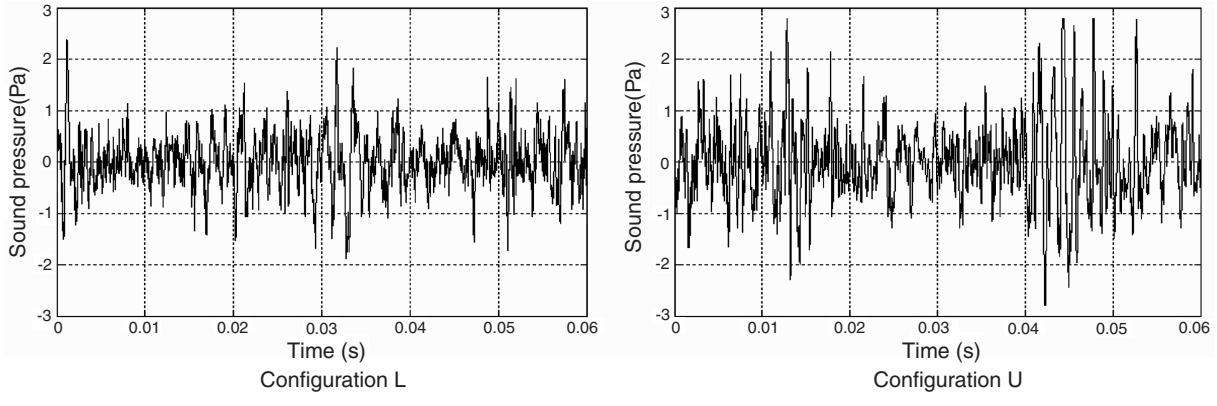

Fig. 10 Comparisons of measured sound pressure time histories for configurations L and U at $\Delta\psi_s = 30$ deg.

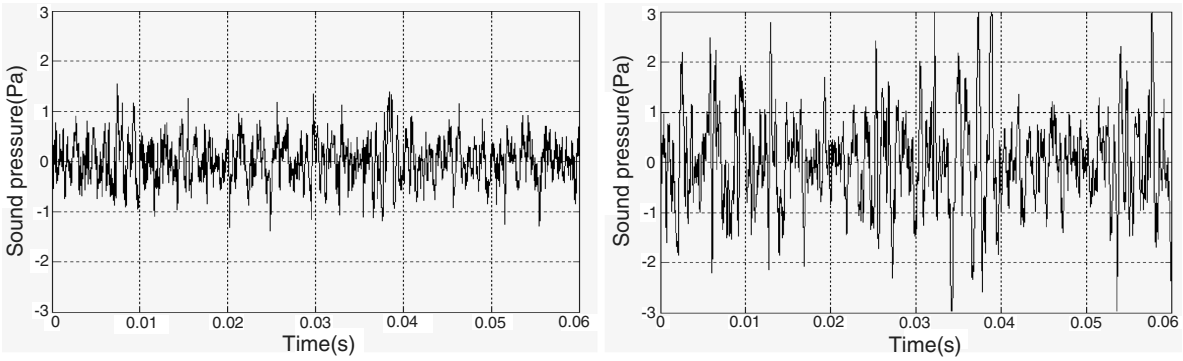

a) n=1000 rpm **b) n=1200 rpm**

Fig. 11 Comparisons on sound pressure time histories for different rotor speeds on observing point 3.

the tip Mach number is one of the important parameters affecting rotor noise levels.

Figure 11 gives the sound pressure time histories for configuration L on observing point 3 for two different rotor speeds. As seen from the figures, the sound pressure amplitude is higher at 1200 rpm than at 1000 rpm.

V. Conclusions

In this study, experiments were carried out to study the aerodynamic and acoustic characteristics of a model scissors rotor. Based on the results shown in this study, the following conclusions can be drawn:

1) The noise level of a scissors rotor with a nonuniform blade azimuthal spacing and a nonzero vertical separation is not always less than that for a conventionally configured rotor with zero vertical separation and uniform blade azimuthal spacing. For some scissors rotor configurations, the vertical separation may cause stronger BVI and therefore higher noise levels than a conventionally configured rotor.

2) At some scissors angles, the scissors rotor with vertical separation may lead to serious blade-vortex interaction due to the close encounter of tip vortices from the blades of the upper rotor and the lower rotor. If strong BVI occurs, the noise levels of the scissors rotor will remarkably increase.

3) The noise levels and characteristics of a scissors rotor are different for configuration L and configuration U due to different BVI possibilities, and the noise for configuration U is larger when compared with configuration L at the present test operating condition.

4) At the operating condition in the current experiment settings, the noise level of the noncoplanar "scissors" rotor with $\Delta\psi_s = 90$ deg is larger than that of the conventional and coplanar rotor.

5) The time-averaged induced velocity near the lower blades of a scissors rotor is consistently larger than that near the upper blades for both configurations, except at the tip region.

6) The tip Mach number is an important parameter in determining the scissors rotor noise level, and the noise level increases rapidly with an increase in the tip Mach number.

Acknowledgments

The authors would like to acknowledge the help extended by Qiang Zhang, Xiao-Lin Zhu, Wei-Sheng Mei, and Ning-Hang Peng et al. of the Nanjing University of Aeronautics and Astronautics in the present experiments. Special thanks to Jinggen Zhao of the Advanced Rotorcraft Technology for his helpful suggestions and discussions.

References

[1] Amer, K. B., and Prouty, R, W., "Technology Advances in the AH-64 Advanced Attack Helicopter," *Vertica*, Vol. 8, No. 2, 1984, pp. 133–164.

[2] Xu, G. H., Wang, S. C., and Zhao, J. G., "Experimental and Analytical Investigation on Aerodynamics of Helicopter Scissors Tail Rotor," *Chinese Journal of Aeronautics*, Vol. 14, No. 4, 2001, pp. 193–199.

[3] Sonneborn, W. G. O., and Drees, J. M., "The Scissors Rotor," *Journal of the American Helicopter Society*, Vol. 20, No. 3, 1975, pp. 18–27.

[4] Rozhdestvensky, M. G., "Scissors Rotor Concept: New Results Obtained," *Presented at the AHS 52nd Annual Forum*, American Helicopter Society, Alexandria, VA, 1996, pp. 1231–1241.

[5] Riley, R. G., "Effects of Uneven Blade Spacing on Ducted Tail Rotor Acoustics," *Presented at the AHS 52nd Annual Forum*, American Helicopter Society, Alexandria, VA, 1996, pp. 1–12.

[6] Brentner, K. S., Edwards, B. D., Riley, R., and Schillings, J., "Predicted Noise for a Main Rotor with Modulated Blade Spacing," *Journal of the American Helicopter Society*, Vol. 50, No. 1, 2005, pp. 18–25.

[7] Johnson, W., "A General Free Wake Geometry Calculation for Wings and Rotors," *Presented at the AHS 51st Annual Forum*, American Helicopter Society, Alexandria, VA, 1995, pp. 137–153.

[8] Bagai, A., and Leishman, J. G., "Rotor Free-Wake Modeling Using a Relaxation Technique-Including Comparisons with Experimental Data," *Journal of the American Helicopter Society*, Vol. 40, No. 3, 1995, pp. 29–41.

[9] Quackenbush, T. R., Boschitsch, A. H., and Wachsprese, D. A., "Fast Analysis Methods for Surface-Bounded Flows with Applications to Rotor Wake Modeling," *Presented at the AHS 52nd Annual Forum*, American Helicopter Society, Alexandria, VA, 1996, pp. 1514–1531.

[10] Xu, G. H., "Investigation on Aerodynamic Characteristics of Helicopter Rotor with New Blade Tip by Free Wake Analysis," Ph.D. Thesis, Nanjing University of Aeronautics and Astronautics, Nanjing, People's Republic of China, 1996 (in Chinese).

[11] Xu, G. H., and Wang, S. C., "An Analytical Method for Predicting Aerodynamic Characteristics of the Rotor with a Swept Tip," *Acta Aerodynamica Sinica*, Vol. 17, No. 3, 1999, pp. 356–361 (in Chinese).

[12] Bagai, A., and Leishman, J. G., "Free-Wake Analysis of Tandem, Tilt-Rotor and Coaxial Rotor Configurations," *Journal of the American Helicopter Society*, Vol. 41, No. 3, 1996, pp. 196–207.

[13] Peng, Y. H., "Investigation on the Blade-Vortex Interaction Aerodynamic Noise of Helicopter Rotors," M.S. Thesis, Nanjing University of Aeronautics and Astronautics, Nanjing, People's Republic of China, 2004 (in Chinese).